Measurement of sub-natural linewidth AC Stark shifts in cold atoms: An experiment for an advanced undergraduate laboratory

J. D. Kleykamp, A. J. Hachtel, D. G. Kane, M. D. Marshall, N. J. Souther, P. K. Harnish, and S. Bali[a)]
Department of Physics, Miami University, Oxford, Ohio 45056-1866

(Received 9 April 2011; accepted 17 August 2011)

We measure sub-MHz AC Stark shifts, also known as light shifts, in an undergraduate laboratory setting using Raman pump-probe spectroscopy to observe sub-natural linewidth spectral features in the transmission spectrum of a weak probe beam passing through a sample of cold 85Rb atoms confined in a magneto-optical trap. To make this observation a pair of inexpensive fast photodiodes and acousto-optic modulators is needed, in addition to equipment commonly found in advanced undergraduate optics labs with laser cooling and atom trapping setups. A theoretical description of light shifts accessible to junior and senior-level physics majors is provided. © *2011 American Association of Physics Teachers*.

[DOI: 10.1119/1.3633702]

I. INTRODUCTION

Following a series of seminal pedagogical papers by Wieman and co-workers during the last two decades on laser cooling and atom trapping using frequency stabilized diode lasers,[1–4] an increasing number of upper-level undergraduate teaching labs are introducing students to ultracold atomic samples at temperatures $T \leq 100$ μK, confined in magneto-optical traps.[5] Building and operating a magneto-optical trap teaches students about frequency-narrowed tunable diode lasers, feedback circuitry for laser-locking, light polarization, optical pumping and hyperfine spectroscopy, magnetic field configurations, and aspects of high vacuum technology. Viewing a video of the slowly moving atoms diffusing outward from the trap, obtained by quickly turning off the magnetic field gradient in the trap thereby creating optical "molasses," is stimulates much student interest. Students can also measure the number and temperature of the trapped atoms, and the trap-loading and loss rates as trap diagnostics while building the trap.[2,3,5]

Once the magneto-optical trap is built, other striking and simple measurements can be done on the trapped cold atoms which illustrate basic physics concepts appropriate for upper-level undergraduates. In this paper, we describe how we can measure sub-MHz AC Stark shifts, also known as light shifts, by Raman pump-probe spectroscopy,[6] implemented with the use of two inexpensive fast photodiodes connected to a simple hand-built amplifier circuit and a standard oscilloscope. Also needed is a pair of acousto-optic modulators, which are widely used generic devices in most optics labs, especially where magneto-optical atom trapping is being done.

Raman spectroscopy is a powerful tool for which various implementations at the undergraduate level have been demonstrated.[7–9] Pump-probe spectroscopy, as shown in Fig. 1, refers to the widely used technique[10] of allowing two beams of light (continuous-wave, in our case) to be simultaneously incident on an atomic sample: one, a strong, fixed-frequency pump beam that induces interesting dynamics that we wish to study, and the other, a weak probe beam that is scanned in frequency around that of the pump.

We investigate pump-induced atomic dynamics by examining frequency-dependent absorption or amplification of the probe beam, which arises from Raman transitions between the atomic states. A Raman transition comprises an absorption from one of the ground sublevels to the excited state, followed by emission to a different ground sublevel. This process is sometimes referred to as "stimulated Raman spectroscopy" in the literature because the two-photon process involves an absorption from the pump (or probe) beam followed by a stimulated emission into the probe (or pump) beam, resulting in probe gain (or loss).

Raman pump-probe spectroscopy has been extensively used to extract information on the rich and varied dynamics of cold atoms.[11–13] The use of Raman pump-probe spectroscopy to observe narrow, sub-natural linewidth Raman transitions between light-shifted Zeeman sublevels of cold trapped atoms was demonstrated in Refs. 14–16. Sub-natural linewidth spectral features are observable because the method relies on stimulated, not spontaneous, transitions, which is the same underlying reason laser linewidths can be much narrower than the natural linewidth of the atoms in the gain medium.

The measurement described in this paper has three important pedagogical benefits. Students learn the physics of light shifts, a fundamental concept in light-atom interactions. This concept is also important in applications such as in the implementation of atomic clocks where light shifts are a principal source of noise.[17] They also learn the basics of Raman pump-probe spectroscopy, which is an important diagnostic methodology that is used extensively in atomic, molecular, and optical physics. In addition, the students learn how to use this method to observe sub-natural linewidth, sub-MHz atomic spectral features, which is of increasing interest in the undergraduate atomic physics laboratory.[18]

II. THEORY FOR LIGHT SHIFT

The calculation of the light shift for a two-level atom is well known,[19–21] but is typically not taught at the undergraduate, level. For this reason and for completeness, we provide the relevant details. The physics of light shifts can be understood in terms of wavefunctions without the need to invoke the density matrix formalism because spontaneous emission can be ignored. If we denote the wavefunction for the atom interacting with an incident light field as $\Psi(\vec{r},t)$, the time evolution of the atomic wavefunction Ψ is described by the Schrödinger equation,

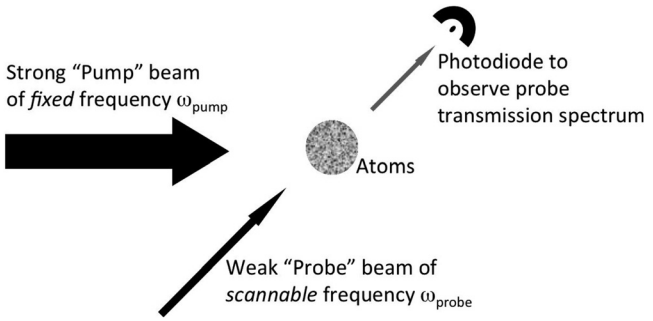

Fig. 1. Basic setup for pump-probe spectroscopy. A strong pump beam of fixed frequency ω_{pump}, together with a weak probe beam for which the frequency ω_{probe} can be scanned around ω_{pump}, are incident on a sample of cold atoms. The probe transmission spectrum is measured.

$$i\hbar\frac{\partial\Psi(\vec{r},t)}{\partial t}=\hat{H}\Psi(\vec{r},t), \tag{1}$$

where $\hat{H}$ is the Hamiltonian of the system. The hat denotes that the Hamiltonian is an operator, acting on the wavefunction Ψ. Because we focus on just the atom and its interaction with the incident field, we may ignore the contribution to the Hamiltonian from the incident field alone (that is, in the absence of the atom, also known as the free field). In that case it is convenient to express $\hat{H}$ as a sum of two terms:

$$\hat{H}=\hat{H}_0+\hat{H}_{\rm int}, \tag{2}$$

where $\hat{H}_0$ is the Hamiltonian for the "bare" atom, that is, in the absence of any external field, and $\hat{H}_{\rm int}$ is the interaction Hamiltonian which describes the interaction between the atom and the external field.

Typically the outermost electrons of the atom are the least tightly bound and respond most readily to the incident field. For this reason alkali atoms are popular because relatively low optical energies are needed to resonantly excite the lone valence electron. Also, the interaction of the single electron with the incident field is simpler to model. The incident electromagnetic field's electric and magnetic vectors, $\vec{E}(\vec{r},t)$ and $\vec{B}(\vec{r},t)$ respectively, interact with the valence electron (negative charge e) through the Lorentz force $\vec{F}$, which in cgs units is $\vec{F}=e(\vec{E}+\vec{v}/c\times\vec{B})$. The electron speed is typically nonrelativistic (that is, $v\ll c$) implying that the effect of the $\vec{B}$ field may be ignored. The $e\vec{E}$ term induces an electric dipole in the atom via displacement of the electron in a direction opposite to that of $\vec{E}$. We denote this induced dipole moment as $\vec{d}$. Thus, $\hat{H}_{\rm int}$ is given by the potential energy stored in the induced dipole,

$$\hat{H}_{\rm int}=-\vec{d}\cdot\vec{E}(\vec{r},t)\approx-\vec{d}\cdot\vec{E}(t). \tag{3}$$

The spatial dependence in the incident electric field has been ignored because the optical wavelength is much larger than the size of the atom (known as the "long wavelength approximation.")

A. Light shift calculation for two-level atoms

For a simple two-level atom as shown in Fig. 2(a), with ground state $|g\rangle$ and excited state $|e\rangle$, we denote the bare energies as E_g and E_e, respectively, where $\hbar\omega_{eg}\equiv E_e-E_g$. The eigenstates of the bare Hamiltonian $\hat{H}_0$ are $|g\rangle$ and $|e\rangle$, that is,

$$\hat{H}_0|g\rangle=E_g|g\rangle,\quad \hat{H}_0|e\rangle=E_e|e\rangle, \tag{4}$$

and may be defined to form an orthonormal basis

$$\langle g|e\rangle=\langle e|g\rangle=0,\qquad \langle g|g\rangle=\langle e|e\rangle=1. \tag{5}$$

An arbitrary wavefunction of the two-level atom, such as $\Psi(\vec{r},t)$ in Eq. (1), may be expressed as a linear superposition of $|g\rangle$ and $|e\rangle$

$$\Psi(\vec{r},t)=a_g(t)|g\rangle+a_e(t)|e\rangle, \tag{6}$$

where the a-coefficients carry the time-dependence and the spatial dependence is carried in $|g\rangle$ and $|e\rangle$. If we substitute Eq. (6) into Eq. (1), choose $E_g=0$, and project the resultant equation first onto $\langle g|$ and next onto $\langle e|$, we obtain, respectively,

$$i\hbar\dot{a}_g=a_gE_g+a_e\langle g|\hat{H}_{\rm int}|e\rangle, \tag{7a}$$

$$i\hbar\dot{a}_e=a_eE_e+a_g\langle e|\hat{H}_{\rm int}|g\rangle, \tag{7b}$$

where we have used Eqs. (4) and (5).

Because $|g\rangle$ and $|e\rangle$ are states of well-defined parity, the form of $\hat{H}_{\rm int}$ in Eq. (3) enables us to use $\langle g|\hat{H}_{\rm int}|g\rangle=\langle e|\hat{H}_{\rm int}|e\rangle=0$. To evaluate the transition matrix elements in Eq. (7) we assume the incident field is a monochromatic wave of frequency ω_L, amplitude E_0, and polarization $\vec{\epsilon}$, that is,

$$\vec{E}(\vec{r},t)=\frac{1}{2}(\vec{\epsilon}E_0e^{-i\omega_Lt}+\text{c.c.}), \tag{8}$$

where $\vec{E}$ is assumed to be spatially uniform over the size of the atom due to the long wavelength approximation, and c.c. denotes complex conjugate. We thus have from Eq. (8),

$$\langle e|\hat{H}_{\rm int}|g\rangle=-\frac{1}{2}\langle e|\vec{d}|g\rangle\cdot(\vec{\epsilon}E_0e^{-i\omega_Lt}+\text{c.c.}), \tag{9a}$$

$$=-\frac{1}{2}\hbar(\chi e^{-i\omega_Lt}+\text{c.c.}), \tag{9b}$$

where $\chi\equiv\langle e|\vec{d}|g\rangle\cdot\vec{\epsilon}E_0/\hbar$ is the Rabi frequency (which, for on-resonance excitation, $\omega_L=\omega_{eg}$, turns out to be the frequency at which the probability of the atom being in the

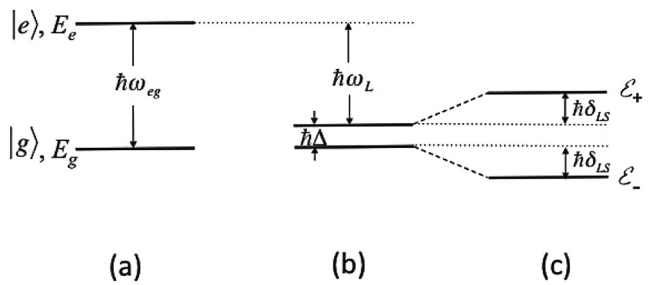

Fig. 2. (a) The eigenstates for the bare atom, without light present. (b) The eigenstates for the bare atom, with zero light excitation, in the rotating wave approximation [$\chi=0$ in Eq. (16)]. These eigenstates are a better basis for describing the atom when, eventually, the atom is illuminated by light. (c) Atom, for nonzero light excitation, in the rotating wave approximation as given by Eq. (16).

excited or ground states oscillates between the two levels). We substitute Eq. (9) into Eq. (7) and obtain

$$i\dot{a}_g = -\frac{1}{2}a_e(\chi e^{-i\omega_L t} + \text{c.c.}), \tag{10a}$$

$$i\dot{a}_e = a_e\omega_{eg} - \frac{1}{2}a_g(\chi e^{-i\omega_L t} + \text{c.c.}). \tag{10b}$$

To solve these differential equations, we take a cue from the solutions obtained for no incident field ($\chi = 0$). In that case, $a_g(t) = a_g(0)$ and $a_e(t) = a_e(0)\exp(-i\omega_{eg}t)$. When $\chi \neq 0$ we expect the driving frequency ω_L, not ω_{eg}, to dominate for long times. Thus, we expect $a_e(t) = c_e(t)\exp(-i\omega_L t)$ where the coefficient c_e is allowed to retain a slow time dependence unlike $a_e(0)$ in the $\chi = 0$ case. For $\chi \neq 0$ we can no longer use $a_g(t) = a_g(0)$, and write it as $c_g(t)$ instead. We obtain

$$i\dot{c}_g = -\frac{1}{2}c_e e^{-i\omega_L t}(\chi e^{-i\omega_L t} + \text{c.c.}), \tag{11a}$$

$$i\dot{c}_e = (\omega_{eg} - \omega_L)c_e - \frac{1}{2}c_g e^{i\omega_L t}(\chi e^{-i\omega_L t} + \text{c.c.}). \tag{11b}$$

We now invoke the rotating wave approximation (RWA) which allows us to ignore terms that oscillate at twice the optical frequency because measurements typically last at least a few optical cycles and such terms would average to zero over time. We let the $\Delta \equiv \omega_{eg} - \omega_L$ and obtain the useful equations:

$$i\dot{c}_g = -(\chi^*/2)c_e, \tag{12a}$$

$$i\dot{c}_e = \Delta c_e - (\chi/2)c_g. \tag{12b}$$

A convenient method for solving Eq. (12) is to express it in the matrix form

$$\begin{pmatrix} i\hbar\dot{c}_g \\ i\hbar\dot{c}_e \end{pmatrix} = \begin{pmatrix} 0 & -\hbar\chi^*/2 \\ -\hbar\chi/2 & \hbar\Delta \end{pmatrix}\begin{pmatrix} c_g \\ c_e \end{pmatrix}. \tag{13}$$

We see that Eq. (13) is a restatement of the Schrodinger equation, Eq. (1), in the rotating wave approximation, that is,

$$i\hbar\frac{\partial}{\partial t}\Psi_{\text{RWA}} = \hat{H}_{\text{RWA}}\Psi_{\text{RWA}}, \tag{14}$$

where, in analogy to Eq. (6), we have defined the wave function $\Psi_{\text{RWA}} \equiv c_g|g\rangle + c_e|e\rangle$, and the operator $\hat{H}_{\text{RWA}}$ is defined by the 2×2 matrix in Eq. (13).

The new stationary energy states for the atom interacting with light are found by evaluating the eigenvalues of the matrix operator H_{RWA}. We denote these new energy states by $\mathcal{E}$ and find that they satisfy the quadratic equation

$$\mathcal{E}(\hbar\Delta - \mathcal{E}) + \frac{\hbar^2|\chi|^2}{4} = 0, \tag{15}$$

which is easily solved for the roots

$$\mathcal{E}_\pm = \frac{\hbar}{2}(\Delta \pm \Omega'), \tag{16}$$

where $\Omega' \equiv \sqrt{\Delta^2 + |\chi|^2}$ is the generalized Rabi frequency.

For zero excitation, $\chi = 0$, the eigenvalues corresponding to Ψ_{RWA} in Eq. (14) are obtained by setting $\chi = 0$ in Eq. (16), and are shown in Fig. 2(b).

Prior to interacting with the incident light field the energy of the ground state is, by definition, zero. For non-zero excitation, Eq. (16) yields a symmetrical light-shift, also known as the AC Stark shift, equal to $\mathcal{E}_+$ and $\mathcal{E}_-$. This light shift is indicated by $\hbar\delta_{\text{LS}}$ in Fig. 2(c). Our discussion will center around the ground state light shift $\mathcal{E}_-$, which has magnitude $\hbar\delta_{\text{LS}}$.

B. Transition from two-level to multi-level atoms

We discuss the transition to a multi-level atom, simplified from Ref. 16. In a real multi-level atom we need to take into account the relative strength of the different transitions, embodied by the Clebsch-Gordan coefficients. In our case the transitions of interest are the Zeeman sublevels of the transition $F_g = 3 \leftrightarrow F_e = 4$ in ^{85}Rb, where F denotes the hyperfine quantum number and includes the electron orbital angular momentum, the electron spin, and the nuclear spin. However, five of the seven Zeeman ground sub-levels lie rather close to each other, and may be approximated as one.[16] Thus, for the purpose of this discussion, we choose the simplest atomic model necessary to explain our Raman pump-probe data, namely a $F_g = 1 \rightarrow F_e = 2$ atom (see Fig. 3).

The light shift, in units of frequency, for any one of the three Zeeman ground states $m_F(-1 \leq m_F \leq 1)$ is given by

$$\delta_{\text{LS}m_F} = \frac{\Gamma}{2}\left(\frac{\Delta}{\Gamma} - \sqrt{\frac{\Delta^2}{\Gamma^2} + \frac{I}{2I_{\text{sat}}}}\right)|c_{m_{F_g}m_{F_e}}|^2, \tag{17}$$

where we have incorporated into Eq. (16) the Clebsch-Gordan coefficient $c_{m_{F_g}m_{F_e}}$ for the transition between the ground state m_{F_g} and the excited state m_{F_e}. For convenience we have written the Rabi frequency χ in terms of measurable quantities I (the laser intensity) and I_{sat} (the saturation intensity for the hyperfine transition, which is defined as the intensity at which the probability of the atom being in the excited state is 1/4) via the relation $I/I_{\text{sat}} \equiv 2|\chi|^2/\Gamma^2$, where Γ is the natural linewidth for the transition. For 85Rb, $I_{\text{sat}} = 1.64$ mW/cm^2 and $\Gamma/2\pi = 5.98$ MHz.[22] The values of the squared Clebsch-

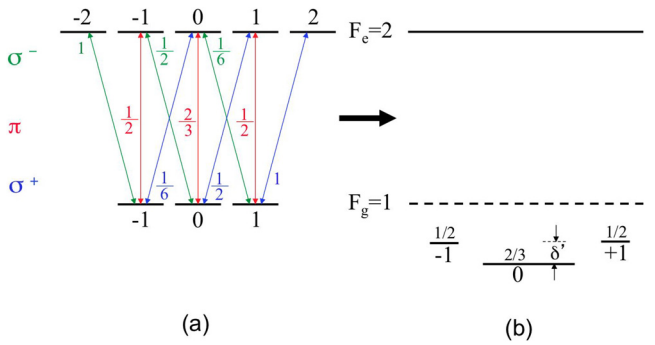

Fig. 3. (Color online) (a) Values of the squared Clebsch-Gordan coefficients for all possible transitions between the Zeeman sublevels of the $F_g = 1 \leftrightarrow F_e = 2$ transition. The notation π, σ^+ and σ^- refer to polarization of the incident light being linear, right- and left-circularly polarized, respectively. (b) The quantity δ' is the relative light shift between the lowest $m_{F_g} = 0$ Zeeman sublevel and the $m_{F_g} = \pm 1$ ground state sublevels, as indicated. If the excitation is π-polarized, the predicted light shifts for the ground Zeeman sublevels are proportional to the indicated values.

Gordan coefficients for all transitions that can be excited by incident light of all possible polarizations between the Zeeman sublevels of the $F_g = 1 \leftrightarrow F_e = 2$ transition are shown in Fig. 3(a).

The relative light shift between the ground states is denoted by δ' as shown in Fig. 3(b). If we assume the incident intensity to be linearly polarized, we can calculate the value of δ' by first substituting $2/3$ for the value of $|c_{m_{F_g} m_{F_e}}|^2$ in Eq. (17) to determine the light shift of the lowest Zeeman sublevel ($m_F = 0$), and then substituting $1/2$ to determine the light shift of the upper ground state sublevels ($m_F = \pm 1$), and taking the difference of the two light shifts. We have

$$\delta' \equiv (\delta_{\mathrm{LS}})_{m_F=0} - (\delta_{\mathrm{LS}})_{m_F=\pm 1}. \tag{18}$$

III. MEASUREMENT OF THE LIGHT SHIFT IN COLD ATOMS USING RAMAN PUMP-PROBE SPECTROSCOPY

We will omit details[16] that are of interest to a more specialized audience and present the main results. New information that is relevant for undergraduate students has been included. As shown in Fig. 4, our experimental setup uses a standard vapor-loaded $\sigma^+ - \sigma^-$ ^{85}Rb magneto-optical trap in a stainless-steel vacuum chamber with anti-reflection coated windows. The 780 nm light from an external cavity tunable diode laser is divided into three mutually orthogonal beams (not shown), each of which is retroreflected, to form a laser trap.

A secondary beam from the same laser is utilized to lock the laser to a hyperfine atomic transition by saturated absorption spectroscopy. The purpose of acousto-optic modulator AO1 in Fig. 4 is to detune the locked laser frequency to any specific frequency that lies within a range of a few natural linewidths from atomic resonance. In our case the trap laser is detuned 2.5 Γ below resonance. The sum of the power of all six trapping beams (15 mm in diameter) at the position of the cold atoms is typically several mW/cm^2 and can be varied with half-wave plate H1 (see Fig. 4). The temperature of the cold atoms is 30–50 μK, and the size of the trapped atom cloud varies between 1 and 3 mm depending on the trap beam intensities. Further details on the magneto-optical trap can be found in Ref. 16.

To detect sub-MHz features using pump-probe spectroscopy, the pump and probe beams are derived from the same laser to preserve the requisite phase coherence.[14] The trapping beams themselves serve as the pump. As shown in Fig. 4, a frequency-scannable probe beam is prepared by passing a small portion of the laser beam through the acousto-optic modulator AO2, and aligning the frequency-shifted output through the second acousto-optic modulator AO3 which is in scanning-mode (that is, a continuously ramping voltage is applied to the "tuning" input of AO3's driver). The frequency-shifted output from AO3 forms the probe beam. The frequency-shifted outputs of AO2 and AO3 are chosen to be of opposite sign so that the probe beam frequency is centered on the original laser (pump frequency, but is capable of scanning around it.

The frequency-shifted output from an acousto-optic modulator shifts spatially when the frequency of the output is varied by changing the tuning voltage, as is the case with AO3. This shift is a problem because the probe beam moves off the trapped atom cloud during the course of its frequency scan. To overcome this problem, the acousto-optic modulator AO3 (and therefore also AO2) is operated in "double-pass" mode as shown in Fig. 5 and described briefly in the following.

The sound wave causes the acousto-optic modulator to act as a diffraction grating producing upshifted (+1) and downshifted (−1) orders, in addition to the 0 order at the incident frequency. In Fig. 5 the −1 order is retroreflected back through the crystal, such that the double-shifted −2 order is aligned with the incident beam but in the counter-propagating direction. This double-shifted beam does not move spatially even as its frequency is tuned. Because the

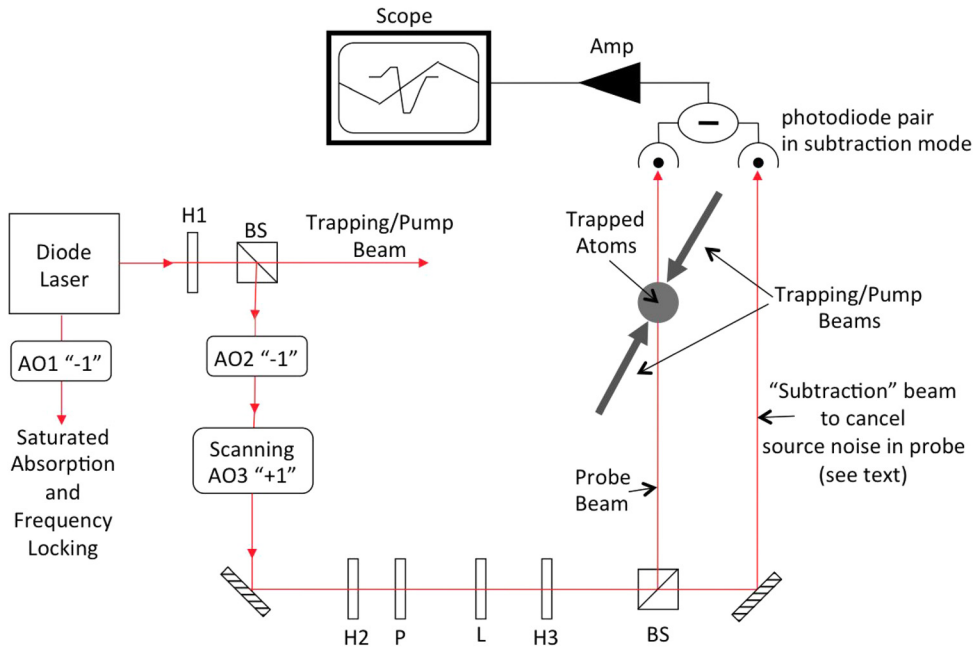

Fig. 4. (Color online) Setup of experiment to measure sub-MHz light shifts in cold atoms using Raman pump-probe spectroscopy. AO = acousto-optical modulator, H = half-wave plate, BS = polarizing beam splitter, L = lens, and P = polarizer. A list of all components, with prices and manufacturers, is in Table 1.

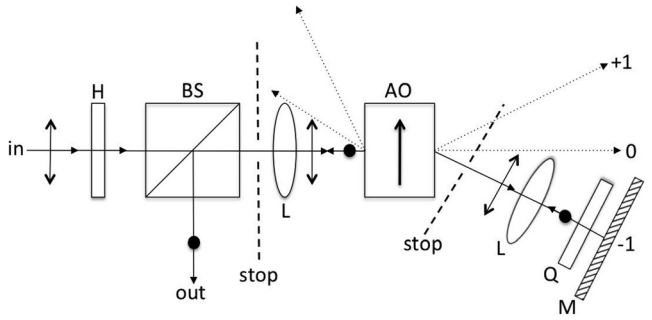

Fig. 5. Creating a frequency scannable probe beam via a double pass through the acousto-optical modulator. L = converging lens of focal length 20 cm, Q = quarter-wave plate, and M = mirror. The arrow inside the AO indicates the direction of propagation of the sound wave through the acousto-optic crystal. See text for further explanation.

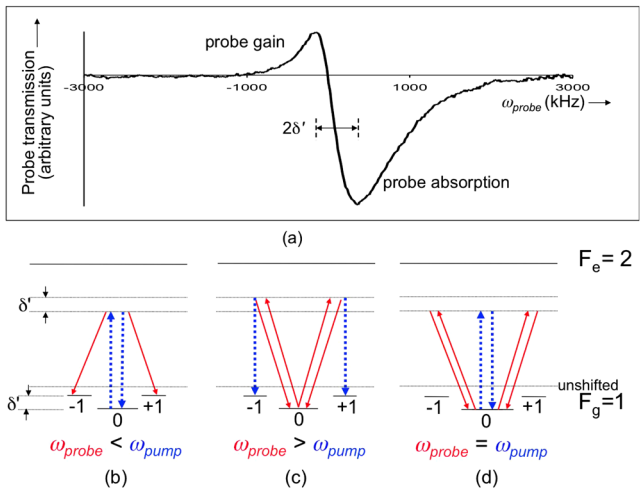

Fig. 6. (Color online) (a) Observed probe transmission spectrum. In (b)–(d) the probe (pump) is denoted by solid (dashed) lines. (b) $\omega_{\text{probe}} < \omega_{\text{pump}}$: absorption from the pump, followed by stimulated emission into the probe, leads to probe gain. (c) $\omega_{\text{probe}} > \omega_{\text{pump}}$: absorption from the probe, followed by stimulated emission into the pump, leads to probe loss. (d) $\omega_{\text{probe}} = \omega_{\text{pump}}$: neither probe gain nor probe loss is observed. [The figure and caption is reproduced from Ref. 16.]

incident polarization is rotated by 90° upon passing twice through Q, the double-shifted, orthogonally polarized output is separated from the incident beam at the polarizing beam splitter BS. The two stops, or pinhole apertures, block the unwanted orders created by the incident beam and the retro-reflected beam. An added advantage of the double-pass scheme is that we obtain double the frequency scan for the same tuning voltage range because the beam makes two passes through the AO.

Next, the frequency-scannable probe is focused with lens L down to a spot of 0.4 mm diameter at the center of the cold atom cloud, with a Rayleigh range much longer than the cloud diameter. The probe beam is linearly polarized by the polarizer P in Fig. 4. The probe intensity can be adjusted without affecting its polarization, with the half-wave plate H2 in Fig. 4, and ranges from 0.03 to 0.5 mW/cm^2 in this experiment. The frequency of the probe beam is scanned at 1.8 MHz/ms for a period of 3.3 ms around the pump frequency. At this detuning and intensity the probe is too weak to visibly exert any forces on the atoms, and is therefore allowed to always be incident on the atomic cloud. The half-wave plate-beam splitter combination H3 followed by the polarizing beam splitter BS in Fig. 4 is used to split the probe into two beams of equal intensity, one of which passes through the cold atoms while the other passes close to the atoms but not through them. The two beams are allowed to fall onto a pair of photodiodes (see Table 1) whose outputs are subtracted (that is, the cathode of one photodiode is tied to the anode of the other) to eliminate noise in the probe beam that originates in the laser. The subtracted output is amplified[24] to yield a transmission spectrum that can be observed on an oscilloscope.

IV. RESULTS AND DISCUSSION

A typical transmission spectrum for the probe beam, as observed directly on a standard oscilloscope, is shown in Fig. 6(a). The curve shown is an average over 5–10 frequency scans. The entire spectrum fits within a frequency range of ~2 MHz, with the frequency separation between the peak and the dip being less than a MHz. The pump intensity needs to be carefully measured, taking into account absorptive losses through the background atomic vapor in the magneto-optical trap and other losses.[16] In the undergraduate lab we simply estimate the pump intensity by measuring the trap laser intensity before it is split into three mutually orthogonal trapping beams, and then doubling this value to take into account the fact that the beams are retroreflected.

We see in Fig. 6(a) that probe gain and absorption are observed as the probe frequency is varied through the pump frequency. As we will explain, we interpret these probe gain and absorption features in terms of stimulated Raman transitions between the light-shifted Zeeman ground sub-levels depicted in Fig. 3(b). For a simple fictitious $F_g = 1 \rightarrow F_e = 2$ atom, we find that gain and loss features occur when the probe is shifted by δ' below and above the pump frequency, respectively. Recall from Fig. 3 that δ' is the relative difference of light shifts between the ground-state Zeeman sub-

Table I. Components used in sub-natural linewidth light shift measurement.

Description	Model	Cost
Acousto-optic modulators	Isomet, driver D322B-805 and crystal 1205C-2-804B or Crystal Technology, driver AODR 1080 AF-AEF0-1.0, and crystal AOMO 3080-122	$1125/$995 $1075 for 1/$1750 for 2, and $1050 for 1/$1200 for 2
Half- and quarter-wave plates	Thorlabs WPMH05M-780 and WPMQ05M-780	$227 each
Polarizers	Edmund Optics N47-215	$100 each
Polarizing beamsplitters	Thorlabs PBS102	$171 each
Mirrors	gold, Edmund Optics N45-606	$60 each
Photodiodes	Hamamatsu S1336-18BK	$18.90 each

levels $m_{F=0}$ and $m_{F=\pm1}$. For the real $F_g=3 \rightarrow F_e=4$ ^{85}Rb atom, the situation is more complicated, leading to the asymmetrical shape of the observed gain-loss curve. We will use the simple $F_g=1 \rightarrow F_e=2$ model to understand in broad terms the origin of the probe gain and loss, as illustrated in Figs. 6(b)–6(d).

The atoms predominantly reside in the lowest ground state ($|F_g=1, m_F=0\rangle$ in Fig. 3, which we denote as $|1,0\rangle$). Hence, we only consider absorption out of that state. The pump is formed by counter-propagating circularly-polarized magneto-optical trap beams. As is well known the polarizations of the beams comprising each counter-propagating pair are orthogonal to each other, leading to a net linear polarization that rotates in space.[23] Thus, if we switch to a reference frame that rotates with the net polarization, the pump appears π-polarized. The probe (which is linearly polarized in the lab frame) then appears to have π as well as right-circularly (σ^+) and left-circularly (σ^-) components. We will show that, in conjunction with the π-polarized pump, the σ^+ and σ^- components of the probe give rise to Raman transitions between the light-shifted levels as depicted in Figs. 6(b)–6(d). The π-polarized component of the probe cannot cause a transfer of population from one ground-state sublevel to another in this model system, and is therefore ignored.

When $\omega_{\text{probe}} < \omega_{\text{pump}}$, the pump is closer to resonance with the excited state and thus is far more likely than ω_{probe} to excite the atoms from the $|1,0\rangle$ state to the $|F_e=2, m_F=0\rangle$ excited state ($|2,0\rangle$ in Fig. 3) because ω_{pump} is π-polarized, and then by stimulated emission back into the pump to the $|1,0\rangle$ state. As ω_{probe} approaches $\omega_{\text{pump}} - \delta'$, the excited atoms are increasingly induced by the σ^+ and σ^- components of the probe to make a stimulated emission into the probe beam and drop from $|2,0\rangle$ to the $|1,\pm1\rangle$ ground states (that is, the $|F_g=1, m_F=\pm1\rangle$ states in Fig. 3). This absorption from the pump followed by stimulated emission into the probe causes a gain in the transmitted probe power, as shown in Fig. 6(a). Note that the probe gain is maximum when $\omega_{\text{probe}} = \omega_{\text{pump}} - \delta'$.

In contrast, as ω_{probe} becomes larger than ω_{pump}, the probe becomes closer to resonance with the excited state and thus is much more likely than the pump to excite the atoms in the $|1,0\rangle$ state to the excited state (that is, to $|2,\pm1\rangle$ and then, by stimulated emission back into the probe, to the $|1,0\rangle$ state again. As shown in Fig. 6(c), when ω_{probe} approaches $\omega_{\text{pump}} + \delta'$, the excited atoms are increasingly induced by the pump to make a stimulated emission into the pump beam and drop from $|2,\pm1\rangle$ to the $|1,\pm1\rangle$ ground states. This absorption from the probe and stimulated emission into the pump causes a loss in the transmitted probe power. The probe loss is maximum when $\omega_{\text{probe}} = \omega_{\text{pump}} + \delta'$.

In between, when $\omega_{\text{probe}} = \omega_{\text{pump}}$, neither ω_{probe} nor ω_{pump} are efficiently tuned to cause stimulated emission from the excited state to the $|1,\pm1\rangle$ states. As shown in Fig. 6(d), both the pump and the probe are equally likely to excite the atom to the excited state $|2,0\rangle$ for the pump and $|2,\pm1\rangle$ for the probe), and by stimulated emission into themselves, back into the $|1,0\rangle$ state. Therefore, the transmitted probe beam shows neither gain nor loss.

We see that measuring the frequency separation between the centers of the probe gain and loss features in Fig. 2(a) yields twice the value of δ'_{LS}, the relative light shift between the ground state Zeeman sublevels [see Eqs. (17) and (18)].

The solid line in Fig. 7 is a plot of the measured relative light shift δ'_{LS} as a function of the pump intensity for magneto-optically trapped 85Rb atoms; the dashed line shows the theoretical prediction by Eqs. (17) and (18) for δ'_{LS}.

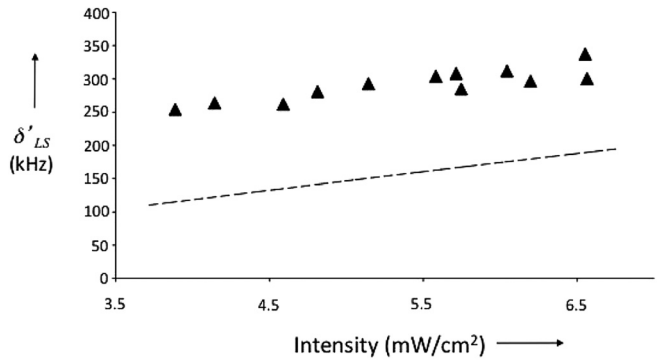

Fig. 7. Sub-MHz, sub-natural linewidth, light shifts (in combination with residual Zeeman shifts) for magneto-optically trapped 85Rb atoms. The solid line is the measurement from Fig. 6 and the dashed line is the theory predicted by Eqs. (17) and (18). The natural linewidth for 85Rb atoms in this experiment is taken to be 6 MHz.

The observed light shifts are all under half a MHz for the achievable range of intensities. Lower pump intensity caused the magneto-optical trap to no longer be able to trap any atoms, and higher pump intensity is not possible with our current setup. Although the observed light shifts vary with the intensity in Fig. 7 in approximately the manner predicted by the theory, there is a more or less constant offset of about 100–150 kHz between the observed (solid line) and predicted values (dashed line). The dominant systematic error in the measurement arises from the pump detuning, which although stable and accurately reproducible, may be different from the expected value by up to $\pm 10\%$.[16] However, this lack of certainty of the pump detuning value leads only to a maximum error of ± 25 kHz, significantly less than the discrepancy observed between measurement and theory. This discrepancy is due to residual Zeeman shifts caused by the magnetic gradient in the magneto-optical trap,[16] which we do not discuss here because it is beyond the scope of the undergraduate laboratory. Reference 16 discusses how to suppress the residual Zeeman shifts to bring the data in agreement with the predictions. The data shown in Fig. 7 are partially reproduced from Fig. 4 in Ref. 16. Students may wish to refer to Ref. 16 for more data and a rigorous explanation. The main point is that Fig. 7 shows that sub-MHz light shifts can be predicted and observed in an undergraduate setting.

ACKNOWLEDGMENTS

The authors gratefully acknowledge invaluable discussions with Lynn Johnson in the Instrumentation Laboratory at Miami University, and with Mike Eldridge. Financial support from the Petroleum Research Fund is gratefully acknowledged. They are indebted to the Dean of the College of Arts and Science at Miami University for generous seed funding for the optics teaching lab for undergraduates and first-year graduate students. They also wish to thank an anonymous referee for extensive suggestions that helped improve the manuscript significantly.

[a]Electronic mail: balis@muohio.edu

[1]K. B. MacAdam, A. Steinbach, and C. Wieman, "A narrow-band tunable diode laser system with grating feedback, and a saturated absorption spectrometer for Cs and Rb," Am. J. Phys. **60**, 1098–1111 (1992).

[2]C. Wieman, G. Flowers, and S. Gilbert, "Inexpensive laser cooling and trapping experiment for undergraduate laboratories," Am. J. Phys. **63**, 317–330 (1995).
[3]S. L. Gilbert and C. Wieman, "Laser cooling and trapping for the masses," Opt. Photonics News **4**, 8–14 (1993).
[4]C. Wieman and L. Hollberg, "Using diode lasers for atomic physics," Rev. Sci. Instrum. **62**, 1–20 (1991).
[5]See, for example, A. S. Mellish, and A. C. Wilson, "A simple laser cooling and trapping apparatus for undergraduate laboratories," Am. J. Phys. **70**, 965–971 (2002).
[6]See, for example, S. Mukamel, *Principles of Nonlinear Optical Spectroscopy* (Oxford U. P., New York, 1995), pp. 321–345.
[7]W. R. C. Somerville, E. C. Le Ru, P. T. Northcote, and P. G. Etchegoin, "High performance Raman spectroscopy with simple optical components," Am. J. Phys. **78**, 671–677 (2010).
[8]B. L. Sands, M. J. Welsh, S. Kin, R. Marhatta, J. D. Hinkle, and S. B. Bayram, "Raman scattering spectroscopy of liquid nitrogen molecules: An advanced undergraduate physics laboratory experiment," Am. J. Phys. **75**, 488–495 (2007).
[9]A. Singha, P. Dhar, and A. Roy, "A nondestructive tool for nanomaterials: Raman and photoluminescence spectrosocpy," Am. J. Phys. **73**, 224–233 (2005).
[10]D. A. Smith and I. G. Hughes, "The role of hyperfine pumping in multilevel systems exhibiting saturated absorption," Am. J. Phys. **72**, 631–637 (2004).
[11]G. Grynberg and C. Robilliard, "Cold atoms in dissipative optical lattices," Phys. Rep. **355**, 335–451 (2001), and references therein.
[12]T. Brzozowski, M. Brzozowska, J. Zachorowski, M. Zawada, and W. Gawlik, "Probe spectroscopy in an operating magneto-optical trap: The role of Raman transitions between discrete and continuum atomic states," Phys. Rev. A **71**, 013401 (2005).
[13]M. Brzozowska, T. Brzozowski, J. Zachorowski, and W. Gawlik, "Nondestructive study of nonequilibrium states of cold trapped atoms," Phys. Rev. A **72**, 061401 (2005).
[14]D. Grison, B. Lounis, C. Salomon, J. Courtois, and G. Grynberg, "Raman spectroscopy of cesium atoms in a laser trap," Europhys. Lett. **15**, 149–154 (1991).
[15]J. Tabosa, G. Chen, Z. Hu, R. Lee, and H. Kimble, "Nonlinear spectroscopy of cold aoms in a spontaneous-force optical trap," Phys. Rev. Lett. **66**, 3245–3249 (1991).
[16]N. Souther, R. Wagner, P. Harnish, M. Briel, and S. Bali, "Measurements of light shifts in cold atoms using Raman pump-probe spectroscopy," Laser Phys. Lett. **7**, 321–327 (2010).
[17]B. H. McGuyer, Y.-Y. Jau, and W. Happer, "Simple method of light-shift suppression in optical pumping systems," Appl. Phys. Lett. **94**, 251110 (2009).
[18]N. Belcher, E. Mikhailov, and I. Novikova, "Atomic clocks and coherent population trapping: Experiments for undergraduate laboratories," Am. J. Phys. **77**, 988–998 (2009).
[19]See, for example, P. W. Milonni and J. H. Eberly, *Laser Physics* (John Wiley & Sons, Hoboken, NJ, 2010) pp. 402–406, from which our treatment up to Eq. (12) is adapted.
[20]See, for example, H. J. Metcalf and P. van der Straten, *Laser Cooling and Trapping* (Springer-Verlag, New York, 1999), pp. 7–8, from which our treatment from Eqs. (13)–(17) is adapted.
[21]For an up-to-date, though more sophisticated, treatment of the light shift, see B. S. Sussman, "Five ways to the nonresonant dynamic Stark effect," Am. J. Phys. **79**, 477–484 (2011), and references therein.
[22]See, for example, Ref. 20, pp. 274–275.
[23]See, for example, Ref. 20, p. 47.
[24]The amplification circuit is straightforward. See, for example, Ref. 1, Fig. 11.